Conformation of Microtubule-Bound Paclitaxel Determined by Fluorescence Spectroscopy and REDOR NMR†

Yankun Li,‡ Barbara Poliks,‡ Lynette Cegelski,‡ Mark Poliks,‡ Zygmunt Gryczynski,§ Grzegorz Piszczek,§ Prakash G. Jagtap,|| Daniel R. Studelska,⊥ David G. I. Kingston,|| Jacob Schaefer,⊥ and Susan Bane*,‡

Department of Chemistry, State University of New York at Binghamton, Binghamton, New York 13902, Department of Chemistry, Washington University, St. Louis, Missouri 63130, Department of Biochemistry and Molecular Biology, Center for Fluorescence Spectroscopy, University of Maryland School of Medicine, Baltimore, Maryland 21201, and Department of Chemistry, Virginia Polytechnic Institute and State University, Blacksburg, Virginia 24061

Received August 19, 1999; Revised Manuscript Received October 25, 1999

ABSTRACT: The conformation of microtubule-bound paclitaxel has been examined by fluorescence and solid-state NMR spectroscopy. A fluorescent derivative of paclitaxel, 3′-*N*-debenzoyl-3′-*N*-(*m*-aminobenzoyl)paclitaxel (*N*-AB-PT), was prepared by semisynthesis. No differences in the microtubule-promoting activity between *N*-AB-PT and paclitaxel were observed, demonstrating that addition of the amino group did not adversely affect the ligand−receptor association. The distance between the fluorophore *N*-AB-PT and the colchicine binding site on tubulin polymers was determined through time-resolved measurements of fluorescence resonance energy transfer to be 29 ± 2 Å. The absorption and emission spectra of *N*-AB-PT bound to microtubules and in various solvents were measured. A plot of the Stokes shift as a function of solvent polarity was highly unusual. The Stokes shift increased linearly with solvent polarity in protic solvents, which is expected due to the nature of the fluorophore. In aprotic solvents, however, the Stokes shift was invariant with solvent polarity, indicating that the fluorophore was somehow shielded from the effects of the solvent. These data are best explained by considering the solution-state conformational properties of paclitaxel. It is known that paclitaxel adopts different conformations depending on the nature of the solvent, and these fluorescence data are consistent with the molecule adopting a "hydrophobic collapsed" conformation in protic solvents and an "extended" conformation in aprotic solvents. The Stokes shift of microtubule-bound *N*-AB-PT was within the protic solvent region, demonstrating that microtubule-bound paclitaxel is in a hydrophobic collapsed conformation. Microtubule-bound paclitaxel was also investigated by solid-state NMR. Paclitaxel was labeled with ^{19}F at the para position of the C-2 benzoyl substituent and with ^{13}C and ^{15}N in the side chain. Distances between the fluorine and carbon nuclei were determined by REDOR. The distance between the fluorine and the 3′-amide carbonyl carbon was 9.8 ± 0.5 Å, and the distance between the fluorine atom and the 3′-methine carbon was 10.3 ± 0.5 Å. These spectroscopic data were used in conjunction with molecular modeling to refine the microtubule-bound conformation of paclitaxel and to suggest an alternative orientation of the ligand within the paclitaxel binding site.

Paclitaxel (**1**) (Chart 1) is an important recent addition to the pharmacopoeia. Since its approval in 1992 for the treatment of ovarian cancer, it has become one of the most widely used drugs in the treatment of refractory breast and ovarian cancers (*1*−*5*). The therapeutic effects of paclitaxel appear to be mediated by its association with cellular microtubules (*6*), although very recent information shows paclitaxel binding to Bcl-2 may provide a second pathway to apoptosis (*7*). The mechanism of paclitaxel binding to microtubules has been studied since microtubules were identified as the cellular target for the drug (*6*). The tubulin heterodimer has one high-affinity binding site for paclitaxel when the protein is assembled into microtubules; paclitaxel binds only weakly to the soluble protein (*8*). Paclitaxel microtubules can be formed from very low concentrations of the purified protein and are highly resistant to cold- or calcium-induced disassembly. Low concentrations of paclitaxel can affect microtubule dynamics without affecting the polymer mass. This action of paclitaxel is sufficient to produce apoptosis and may be significant in the drug's therapeutic mechanism (*8*−*11*).

Paclitaxel is a structurally complex molecule. It is prepared commercially by semisynthesis, in which a synthetic side chain is attached to the taxane ring of 10-deacetylbaccatin III, a natural product isolated from needles from *Taxus* plants (*12*). Ideally, future generations of paclitaxel-type drugs would contain the necessary three-dimensional features of paclitaxel without its structural complexity. Rational devel-

† This work was supported by NIH Grants (CA 69571 and CA 55731 to S.B. and D.G.I.K. and GM40634 to J.S.) and an NSF Grant (MCB-9604860 to J.S.).

* To whom correspondence should be addressed. Telephone: (607) 777-2927. Fax: (607) 777-4478. E-mail: sbhastie@binghamton.edu.
‡ State University of New York at Binghamton.
§ University of Maryland School of Medicine.
|| Virginia Polytechnic Institute and State University.
⊥ Washington University.

10.1021/bi991936r CCC: $19.00
Published on Web 12/15/1999

Chart 1

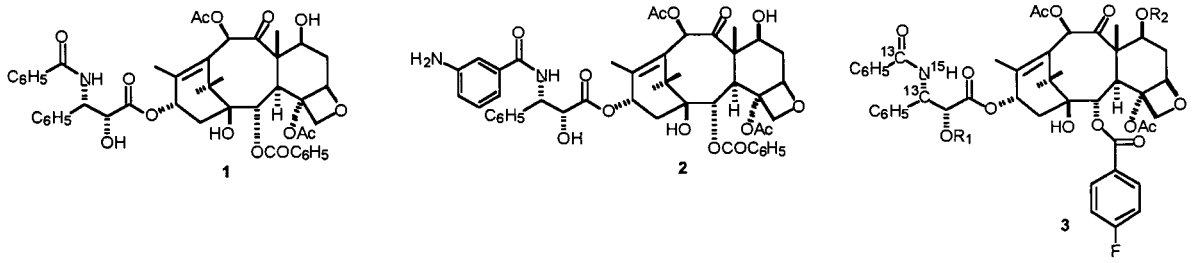

opment of such drugs requires knowledge of the three-dimensional structure of the ligand−receptor complex. The three-dimensional structure of the protein to 3.7 Å resolution was determined by electron crystallography of zinc-induced tubulin sheets containing paclitaxel (*13*). The electron density maps were unfortunately not clear enough in the paclitaxel region to determine definitively the microtubule-bound structure of the drug.

Determination of the structure of the microtubule-bound drug is further complicated by the conformational mobility of the molecule. The taxane ring of paclitaxel and related taxoids is quite rigid, but substituents and the side chain can adopt a variety of different, low-energy conformations (*14*, *15*). The conformations observed thus far can be divided into two general types. One type of conformation is characterized by a clustering of the 3′-PhCONH, 2-benzoate, and 4-acetoxy moieties. This is the "extended" conformation, which is observed in the crystal structure of docetaxel (Taxotere) (*16*) and has been deduced from NMR spectroscopy to be the molecular conformation in apolar solvents (*17*, *18*). In the second type of conformation, the "hydrophobic collapsed" conformation, a clustering of the 3′-phenyl, 2-benzoate, and 4-acetoxy moieties occurs. These hydrophobic collapsed conformations have been observed in the crystal structure of paclitaxel and in protic solvents by NMR (*14*, *17*, *19*, *20*, *23*).

It is well established that elimination of the side chain abolishes the anticancer activity of paclitaxel (*21*−*23*). It therefore appears that determining which of the paclitaxel conformations is the active species will be critical to the development of new drugs. In this report, we have approached the problem spectroscopically. In one series of experiments, a fluorescent derivative of paclitaxel was employed. 3′-*N*-Debenzoyl-3′-*N*-(*m*-aminobenzoyl)paclitaxel (*N*-AB-PT,[1] **2**) was prepared so it could serve as a paclitaxel derivative that would possess fluorescent properties distinct from those of the microtubule but with minimum structural modifications of the parent molecule. In a second series of experiments, we used solid-state NMR methods to determine interatomic distances in an isotopically labeled paclitaxel (2-FB-PT, **3**) bound to microtubules. These two methods are complementary. The NMR method has inherently high resolution, but must be performed on lyophilized microtubules. Fluorescence spectroscopy has much lower resolution, but can be performed on microtubules in solution.

The results from our fluorescence studies demonstrated that the hydrophobic collapsed conformation of paclitaxel best represents the microtubule-bound species. The NMR studies served to further refine the conformation of the microtubule-bound structure. Results from fluorescence resonance energy transfer measurements suggested the relative orientation of paclitaxel in its binding site. Combining the experimental results with the three-dimensional structure of tubulin and molecular modeling methods leads us to propose an alternative structure of paclitaxel within the receptor binding site.[2]

EXPERIMENTAL PROCEDURES

Materials. Colchicine was purchased from U.S. Biochemical Corp. and was recrystallized from ethyl acetate prior to use. Thiocolchicine was prepared from colchicine as previously described (*24*). Paclitaxel derivatives **2** and **3** were prepared by semisynthesis as described briefly below and in more detail in the Supporting Information. The concentrations of *N*-AB-PT (**2**), colchicine, and thiocolchicine were determined spectrophotometrically. Molar absorptivities of these compounds were as follows. For *N*-AB-PT, $\epsilon_{320} = 2.08 \times 10^3\ M^{-1}\ cm^{-1}$ in DMSO and $\epsilon_{313} = 2.33 \times 10^3\ M^{-1}\ cm^{-1}$ in ethanol. For colchicine, $\epsilon_{352} = 1.69 \times 10^4\ M^{-1}\ cm^{-1}$ in PME buffer (*25*). For thiocolchicine, $\epsilon_{398} = 1.7 \times 10^4\ M^{-1}\ cm^{-1}$ in PME buffer (*25*).

All the solvents that were used in the spectral measurements were either spectrograde or freshly purified following standard procedures to remove traces of water. The buffers used in the experiments were as follows: PME, 50 mM PIPES, 0.5 mM $MgSO_4$, and 1 mM EGTA (pH 6.9); PME2, 100 mM PIPES, 2 mM $MgSO_4$, and 2 mM EGTA (pH 6.9); and PMEG, 100 mM PIPES, 1 mM $MgSO_4$, 2 mM EGTA, and 1 mM GTP (pH 6.9).

MAP free bovine brain tubulin was prepared by two cycles of temperature-dependent assembly and disassembly followed by phosphocellulose chromatography (*26*). The purified tubulin was then drop-frozen and stored in liquid nitrogen. Before use, the pellets were thawed and centrifuged

[1] Abbreviations: 2-FB-PT, [^{15}N,3′-^{13}C]-*N*-debenzoyl-*N*-[*carbonyl*-^{13}C]benzoyl-2-debenzoyl-2-(*p*-fluorobenzoyl)paclitaxel; CAN, ceric ammonium nitrate; DMAP, 4-(dimethylamino)pyridine; DMF, *N*,*N*-dimethylformamide; DMSO, dimethyl sulfoxide; EGTA, [ethylenebis-(oxyethylenenitrilo)]tetraacetic acid; EtOAc, ethyl acetate; GTP, guanosine 5′-triphosphate; LDA, lithium diisopropylamide; MAPs, microtubule-associated proteins; MeCN, acetonitrile; *N*-AB-PT, 3′-*N*-debenzoyl-3′-*N*-(*m*-aminobenzoyl)paclitaxel; PIPES, 1,4-piperazinebis(ethanesulfonic acid); PME, 50 mM PIPES, 0.5 mM $MgSO_4$, and 1 mM EGTA (pH 6.9); PME2, 100 mM PIPES, 2 mM $MgSO_4$, and 2 mM EGTA (pH 6.9); PMEG, 100 mM PIPES, 1 mM $MgSO_4$, 2 mM EGTA, and 1 mM GTP (pH 6.9); PMP, *p*-methoxyphenyl; PTLC, preparative thin-layer chromatography; RET, resonance energy transfer; TEA, triethylamine; TES, 2-{[tris(hydroxymethyl)methyl]amino}-1-ethanesulforic acid; THF, tetrahydrofuran; TIPS, triisopropylsilyl trifluoromethanesulfonate.

[2] This work was presented in part at the 38th Annual Meeting of the American Society for Cell Biology, San Francisco, CA, December 1998.

at 5000*g* and 4 °C for 10 min to remove any denatured protein, and then equilibrated into the appropriate buffer. The concentration of tubulin was determined spectrophotometrically using an ϵ_{278} of 1.23 M^{-1} cm^{-1} (*27*).

General Synthetic Methods. [*carbonyl*-^{13}C]Benzaldehyde, [*carbonyl*-^{13}C]benzoic acid, and $^{15}NH_4OH$ were purchased from Cambridge Isotope Laboratories (Cambridge, MA). Other general experimental conditions were as previously described (*28*).

*3′-N-Debenzoyl-3′-N-(m-nitrobenzoyl)-2′-(triisopropylsilyl)paclitaxel (**5**)*. To a solution of **4** (*29*, *30*) (0.065 g, 0.07 mmol) in EtOAc (3 mL) and a 1 N solution of $NaHCO_3$ (5 mL) was added a solution of *m*-nitrobenzoyl chloride (0.020 g, 0.1 mmol) in EtOAc (1 mL). The mixture was stirred at room temperature for 1 h, and diluted with EtOAc. Standard workup followed by purification of the product by PTLC (1000 μM, 6:4 EtOAc/hexane) provided **5** (0.067 g, 89%).

*3′-N-Debenzoyl-3′-N-(m-nitrobenzoyl)paclitaxel (**6**)*. To a solution of **5** (0.065 g, 0.061 mmol) in THF (3 mL) was added HF/pyridine (1 mL), and the mixture was stirred at room temperature for 3 h. It was then diluted with EtOAc, and the organic layer was washed with saturated $NaHCO_3$ solution, water, and brine, dried over Na_2SO_4, and concentrated in vacuo. The residue that was obtained was purified by PTLC (1000 μM, 6:4 EtOAc/hexane) to provide **6** (0.055 g, 100%).

*3′-N-Debenzoyl-3′-N-(m-aminobenzoyl)paclitaxel (**2**)*. A solution of **6** (0.055 g, 0.061 mmol) in MeOH (5 mL) was treated with hydrogen gas (40 psi) in the presence of Pd-C (0.100 g, 10%) at room temperature for 30 min. The reaction mixture was filtered through a pad of Celite and silica gel and washed with EtOAc. The organic layer was concentrated in vacuo, and the residue that was obtained was purified by PTLC (1000 μM, 3:1 EtOAc/hexane) to provide **2** (0.040 g, 75%). ^{1}H NMR: δ 1.13 (s, 3H), 1.23 (s, 3H), 1.68 (s, 3H), 1.72 (s, 1H), 1.79 (s, 3H), 1.84−1.92 (m, 1H), 2.23 (s, 3H), 2.25−2.36 (m, 2H), 2.40 (s, 3H), 2.46 (d, J = 4.12 Hz, 1H), 2.50−2.90 (m, 1H), 3.53 (d, J = 5.19 Hz, 1H), 3.69 (bs, 2H), 3.79 (d, J = 7.17 Hz, 1H), 4.19 (d, J = 8.4 Hz, 1H), 4.30 (d, J = 8.39 Hz, 1H), 4.20 (dd, J = 6.87 and 10.99 Hz, 1H), 4.76−4.78 (dd, J = 2.59 and 5.18 Hz, 1H), 4.94 (d, J = 7.32 Hz, 1H), 5.67 (d, J = 7.17 Hz, 1H), 5.75−5.78 (dd, J = 2.59 and 8.70 Hz, 1H), 6.23 (dd, J = 8.69 and 8.85 Hz, 1H), 6.26 (s, 1H), 6.76 (d, J = 8.85 Hz, 1H), 6.90 (d, J = 9.0 Hz, 1H), 7.03 (m, 2H), 7.16 (dd, J = 8.09 and 8.78 Hz, 1H), 7.34−7.63 (m, 10H), 8.15 (dd, J = 1.52 and 7.02 Hz, 2H). ^{13}C NMR: δ 9.5, 14.8, 20.8, 21.8, 22.6, 26.8, 35.5, 35.6, 43.1, 45.5, 54.9, 58.5, 72.1, 72.3, 73.2, 74.9, 75.5, 79.0, 81.0, 84.3, 113.8, 116.3, 118.2, 126.9, 128.2, 128.7, 128.9, 129.1, 129.5, 130.2, 133.0, 133.7, 134.7, 137.9, 142.0, 166.9, 167.1, 170.3, 171.2, 172.6, 203.6. HR-FABMS: *m*/*z* $[M + H]^+$ 869.3496 (calcd for $C_{47}H_{53}N_2O_{14}$, 869.3495).

*(3R,4S)-[^{15}N,4-^{13}C]-N-(p-Methoxyphenyl)-3-[(triisopropylsilyl)oxy]-4-phenylazetidin-2-one (**9**)*. To a solution of [^{15}N]-*p*-anisidine (*31*, *32*) (**7**, 210 mg, 1.7 mmol) in dichloromethane (10 mL) was added [*carbonyl*-^{13}C]benzaldehyde (180 mg, 1.7 mmol). The mixture was stirred overnight over anhydrous $MgSO_4$ (1 g) at room temperature; the $MgSO_4$ was filtered off, and the filtrate was concentrated in vacuo to give crude **8** (295 mg, 82%), which was used without purification for the next reaction. (3*R*,4*S*)-2-Triisopropylsilyloxy(2-phenylcyclohexyl)acetate (*12*) (190 mg, 0.48 mmol) was coupled with **8** (95 mg, 0.44 mmol) as previously described for the unlabeled compound to give **9** (145 mg, 76%).

*(3R,4S)-[^{15}N,4-^{13}C]-3-[(Triisopropylsilyl)oxy]-4-phenylazetidin-2-one (**10**)*. Azetidinone **9** (145 mg, 0.33 mmol) was oxidized with ceric ammonium nitrate as previously described to give **10** (60 mg, 55%).

*(3R,4S)-[^{15}N,4-^{13}C]-N-[carbonyl-^{13}C]Benzoyl-3-[(triisopropylsilyl)oxy]-4-phenylazetidin-2-one (**11**)*. Acylation of **10** (30 mg, 0.09 mmol) was achieved with [*carbonyl*-^{13}C]-benzoyl chloride (15 mg, 0.1 mmol) in the presence of DMAP (2 mg) and triethylamine (0.1 mL) in methylene chloride (5 mL) at 0 °C. Standard workup and purification by PTLC (silica gel, 1000 μM, 1:5 EtOAc/hexane) gave **11** (24 mg, 62%). ^{1}H NMR: δ 0.89−1.01 (m, 21H), 5.24−5.25 (m, 1H), 5.61 (d, J = 6.1 Hz, 1H), 7.30−7.41 (m, 5H), 7.45−7.49 (m, 2H), 7.49−7.58 (m, 1H), 8.01−8.05 (m, 2H). HR-FABMS: *m*/*z* $[M + H]^+$ 427.2330 (calcd for $C_{23}{}^{13}C_2H_{34}{}^{15}NO_3Si$, 427.2345).

*7,13-Bis(triethylsilyl)-2-debenzoyl-2-(p-fluorobenzoyl)baccatin III (**12**)*. 2-Debenzoyl-7,13-bis(triethylsilyl)baccatin III (*33*) (59 mg, 0.083 mmol) was acylated with *p*-fluorobenzoic acid (232 mg, 1.6 mmol) as previously described for acylation of paclitaxel (*34*) to yield **12** (55 mg, 90% based on 52 mg of unrecovered starting material).

*2-Debenzoyl-2-(p-fluorobenzoyl)baccatin III (**13**)*. Compound **12** (52 mg, 0.062 mmol) was deprotected with HF/pyridine (0.5 mL) to give **13** (28 mg, 75%).

*2-Debenzoyl-2-(p-fluorobenzoyl)-7-(triethylsilyl)baccatin III (**14**)*. Compound **13** (28 mg, 0.046 mmol) was treated with triethylsilyl chloride (40 mL, 0.23 mmol) and imidazole in DMF to yield **14** (28 mg, 84%). ^{1}H NMR: δ 0.53−0.60 (m, 6H), 0.88−0.93 (m, 9H), 1.02 (s, 3H), 1.17 (s, 3H), 1.66 (s, 3H), 1.81−1.90 (m, 1H), 2.16 (s, 3H), 2.17 (s, 3H), 2.17−2.25 (m, 1H), 2.26 (s, 3H), 2.52 (m, 1H), 3.86 (d, J = 6.87 Hz, 1H), 4.12 (d, J = 7.63 Hz, 1H), 4.26 (d, J = 8.09 Hz, 1H), 4.45−4.49 (dd, J = 6.72 and 10.38 Hz, 1H), 4.81 (m, 1H), 4.95 (d, J = 7.94 Hz, 1H), 5.59 (d, J = 7.02 Hz, 1H), 6.44 (s, 1H), 7.11−7.16 (m, 2H), 8.09−8.12 (m, 2H). ^{13}C NMR: δ 5.25, 6.70, 9.90, 14.92, 20.03, 20.90, 22.63, 26.78, 37.18, 38.19, 42.72, 47.21, 58.61, 67.87, 72.30, 74.88, 75.73, 78.72, 80.82, 84.21, 115.69, 115.91, 132.56, 132.61, 132.65, 143.96, 166.06, 169.30, 170.57, 202.08. HR-FABMS: *m*/*z* 741.3115 $[M + Na]^+$ (calcd for $C_{37}H_{51}O_{11}FNaSi$, 741.3082).

*[^{15}N,3′-^{13}C]-N-Debenzoyl-N-[carbonyl-^{13}C]benzoyl-2′-(triisopropyl)-7-(triethylsilyl)-2-debenzoyl-2-(p-fluorobenzoyl)-paclitaxel (**15**)*. To a solution of **14** (14 mg, 0.019 mmol) and **11** (24 mg, 0.055 mmol) in THF (1 mL) was added NaH (38 mg, 50 equiv, 60% dispersion in mineral oil) at 0 °C, and the mixture was stirred at room temperature for 2 h. The reaction was then quenched with AcOH (0.5 mL) at 0 °C and the mixture diluted with EtOAc (5 mL). This reaction mixture was diluted with water and extracted with EtOAc (2 × 10 mL) and the organic layer washed with a saturated solution of $NaHCO_3$, water, and brine followed by drying over Na_2SO_4. The residue obtained after evaporation under reduced pressure was purified by PTLC (silica gel, 1000 μM, 1:3 EtOAc/hexane) to provide **15** (16 mg, 72%).

*[^{15}N,3′-^{13}C]-N-Debenzoyl-N-[carbonyl-^{13}C]benzoyl-2-debenzoyl-2-(p-fluorobenzoyl)paclitaxel (**3**)*. Compound **15** (14 mg, 0.012 mmol) was deprotected with HF/pyridine to give **3** (9.9 mg, 93%). ^{1}H NMR: δ 1.13 (s, 3H), 1.23 (s, 3H),

1.67 (s, 3H), 1.80 (s, 3H), 1.84−1.91 (m, 1H), 2.16 (s, 1H), 2.23 (s, 3H), 2.25−2.36 (m, 1H), 2.39 (s, 3H), 2.48 (d, J = 4.12 Hz, 1H), 2.50−2.58 (m, 1H), 3.49−3.51 (dd, J = 1.98 and 4.88 Hz, 1H), 3.79 (d, J = 7.17 Hz, 1H), 4.18 (d, J = 8.55 Hz, 1H), 4.27 (d, J = 8.39 Hz, 1H), 4.37−4.43 (m, 1H), 4.79−4.81 (dd, J = 2.6 and 5.04 Hz, 1H), 4.94 (d, J = 7.78 Hz, 1H), 5.63 and 5.97 (m each, 2H), 5.64 (d, J = 7.01 Hz, 1H), 6.25 (m, 1H), 6.26 (s, 1H), 6.83 and 7.06 (m each, 2H), 7.16 (t, J = 8.7 Hz, 2H), 7.33−7.52 (m, 9H), 7.70−7.73 (m, 2H), 8.14−8.17 (m, 2H). ^{13}C NMR (^{13}C-labeled peaks in bold): δ 9.54, 14.81, 20.82, 21.87, 22.63, 26.82, 35.53, 35.67, 43.12, 45.56, **54.73**, **54.84**, 58.56, 72.13, 72.31, 72.85, 73.23, 75.13, 75.48, 76.39, 76.66, 76.98, 77.29, 79.16, 81.09, 84.41, 115.86, 116.08, 126.97, 126.99, 128.33, 128.67, 128.71, 129.01, 129.04, 131.97, 132.77, 132.87, 133.08, 142.00, 166.03, **166.92**, **167.06**, 170.28, 171.22, 172.74, 203.53. HR-FABMS: m/z 875.3335 $[M + H]^+$ (calcd for $C_{45}{}^{13}C_2H_{51}{}^{15}NO_{14}F$, 875.3331). The isotopic enrichment determined by mass spectrometry was greater than 95%.

Absorption Spectroscopy. The absorption spectra of *N*-AB-PT in different solvents were obtained using a Hewlett-Packard 8453 diode array spectrometer connected to a personal computer. All measurements were performed in standard mode at ambient temperature. The absorption spectrum of microtubule-bound *N*-AB-PT cannot be obtained directly due to the high turbidity of the solution. We found that the turbidity increase (apparent ΔA at 400 nm) of 10 μM tubulin induced by 10 μM *N*-AB-PT was the same as the turbidity increase of 10 μM tubulin induced by 9 μM paclitaxel. The apparent absorption spectrum of microtubules induced by paclitaxel was therefore measured as the light-scattering reference and was subtracted from the apparent absorption spectrum of microtubules induced by *N*-AB-PT, yielding the net absorption spectrum of microtubule-bound *N*-AB-PT.

Steady-State Fluorescence Spectroscopy. The excitation and emission spectra of *N*-AB-PT in different solvents and bound to microtubules were obtained on a SLM 48000 spectrofluorometer. Excitation spectra were corrected with a rhodamine B solution in the reference channel; emission spectra were uncorrected. A 2 mm × 10 mm quartz cell was used for the measurements and was oriented such that the excitation beam was passing through the smaller path, to minimize any possible inner filter effect. Light scattering due to microtubules was found to be negligible under the experimental conditions that were used. Förster distances between donor and acceptor were determined as previously described for a fluorescent paclitaxel−colchicinoid system (*35*). Quantum yields of 2-AB-PT were determined by comparison to the quantum yield of quinine sulfate in 0.1 M sulfuric acid (*36*).

Frequency-Domain Fluorescence Spectroscopy. Frequency-domain fluorescence experiments were carried out in the Center for Fluorescence Spectroscopy in Baltimore using the instrument described previously (*37*). The excitation source was the cavity-dumped output of a synchronously pumped DCM dye laser, generating a laser pulse train with a repetition rate of 1.85 MHz and a pulse width of about 7 ps. The dye laser output was frequency doubled to 350 nm and used to directly excite the samples, with the donor emission isolated using a 420−280 nm band-pass filter. Distance distributions between the donor and acceptor were recovered from the intensity decay kinetics of the donor (*38*). These determinations were previously performed for a fluorescent paclitaxel−colchicinoid system, and details of the theory and procedures can be found in ref *35*.

Preparation of Tubulin−Ligand Samples for Frequency-Domain Spectroscopy. *(1) Preparation of Tubulin−Colchicine and Tubulin−Colchicine−N-AB-PT*. Tubulin (20 μM) was incubated with a 10-fold excess of colchicine at 37 °C for 30 min in PME buffer. Unbound colchicine was removed by rapid gel filtration (*39*). Tubulin−colchicine prepared this way was then diluted to a final concentration of 5 μM with PME buffer and incubated with 5 μM *N*-AB-PT at ambient temperature for 20 min.

(2) Preparation of Tubulin−Thiocolchicine and Tubulin−Thiocolchicine−N-AB-PT. Tubulin−thiocolchicine and tubulin−thiocolchicine−*N*-AB-PT were prepared in the same manner as described above, except using thiocolchicine instead of colchicine.

Preparation of Tubulin−Ligand Samples for REDOR. Tubulin was prepared in a buffer consisting of 0.1 M ammonium acetate (pH 7.0), 1 mM $MgSO_4$, 0.1 mM GTP, and 0.5% PVP (polyvinyl pyrrolydine). Tubulin was polymerized by 2-FB-PT dissolved in ethanol. The final concentration of protein and of 2-FB-PT was 50 μM; the final concentration of ethanol in the sample was <2%. The solution was distributed among cryovials in 0.5 mL aliquots. Vials containing polymerized tubulin were rapidly frozen by immersion in liquid nitrogen. The frozen samples were immediately transferred to a Thermovac lyophilizer and lyophilized for 3−4 days. A small amount of the lyophilized sample was reconstituted and checked for the presence of microtubules by electron microscopy. The rest of the sample (containing about 75 mg of protein) was packed into the rotor for the REDOR experiment.

REDOR NMR. ^{13}C{^{15}N or ^{19}F} double REDOR (*40*) was performed using a six-frequency transmission-line probe having a 12 mm long, 6 mm inside diameter analytical coil and a Chemagnetics/Varian ceramic stator. Powdered samples were contained in thin-wall Chemagnetics/Varian 5 mm outside diameter zirconia rotors. The rotors were spun at 6250 Hz with the speed under active control to within ±2 Hz. The spectrometer was controlled by a Tecmag pulse programmer. ^{13}C radiofrequency pulses (125 MHz) and ^{15}N radiofrequency pulses (50.7 MHz) were produced by 1 and 2 kW American Microwave Technology power amplifiers, respectively. ^{1}H (500 MHz) and ^{19}F (470 MHz) radiofrequency pulses were generated by 1 kW Creative Electronics tube amplifiers driven by 100 W American Microwave Technology power amplifiers. The π pulse lengths were 10 μs for ^{13}C and ^{15}N and 5 μs for ^{19}F. Distance measurements (*41, 42*) using ^{19}F dephasing were calibrated using the two-bond coupling of [^{19}F]polycarbonate (*43*). Standard XY-8 phase cycling (*44*) was used for REDOR. A 12 T static magnetic field was provided by an 89 mm bore Magnex superconducting solenoid. Proton−carbon cross-polarization transfers were made in 2 ms at 50 kHz. Proton dipolar decoupling was 100 kHz during dipolar evolution and data acquisition.

The key experiment with the quadruply labeled analogue **3** required a total of 3 months of NMR acquisition time to obtain an acceptable signal:noise ratio for one of the REDOR peaks. The data acquisition proceeded as follows. REDOR

Scheme 1

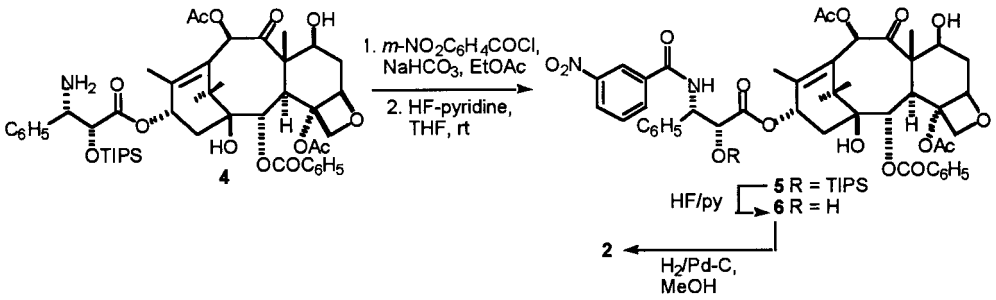

data were collected in twelve 1 week blocks, with each block subdivided into eight segments. If anything that would interfere with the data collection happened during the week (power interruption for a thunderstorm, for example), that segment was discarded. A 1 week block therefore might have taken longer than a week to collect if there were one or two rejections. There were four calibration tests made during the experiment: one at the beginning and one at the end and two during the course of the acquisition, both after power interruptions. The calibration of the spectrometer was unchanged over the entire collection period. The sample temperature was −5 °C throughout.

Attempts were made to reconstitute the sample after the REDOR experiment was completed. The resulting sample could not be adequately dissolved in aqueous solution. The 1 week blocks at the end of the experiment were indistinguishable from those at the beginning, indicating that the sample was not noticeably affected by the long acquisition time.

Computer Modeling. Atomic coordinates of the αβ-tubulin dimer from electron crystallography (*13*) were kindly provided to us by E. Nogales and K. Downing prior to their public release. The taxoid molecule in this structure is docetaxel. The docetaxel was manually converted to paclitaxel by replacing the butoxy group with an aromatic ring and adding an acetyl group at C-10. The missing hydrogens were added to the protein. No solvent was added. The resulting structure (protein with ligand in the binding site) was slowly minimized (following the usual approach to relaxing a crystal-derived protein system) to the derivative of 0.1 kcal mol^{-1} $Å^{-2}$ with distance restraints obtained from REDOR imposed on the two corresponding intramolecular distances.

This form of the tubulin-bound paclitaxel best corresponds to the solution-state conformer found in an aprotic, apolar solution. The conformation of paclitaxel seen in protic solvents was obtained from the X-ray coordinates of paclitaxel in the "Taxol B" conformation (*19*). The coordinates of this structure were placed in the taxoid binding site by using the best visual fit of this structure to the taxane ring system of docetaxel. The resulting structure was minimized as described above. A third orientation of paclitaxel was initiated by "inverting" the Taxol B conformation in the taxoid binding site; the positions of the aromatic rings at C-2 and NHCOPh were interchanged by visual fitting. The resulting structure was minimized as described above. The software programs from MSI (San Diego, CA) were used in all calculations.

Tubulin Assembly. Tubulin assembly was monitored by apparent light scattering using a Hewlett-Packard 8453 diode array spectrometer connected to a personal computer as described previously (*45*).

Scheme 2[a]

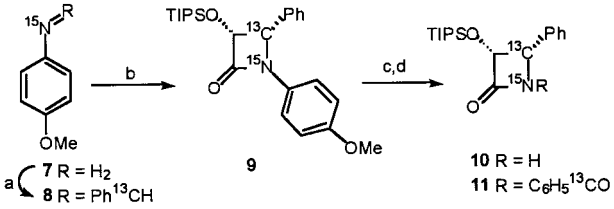

[a] (a) $MgSO_4$, CH_2Cl_2, PhCHO(^{13}CO), 82%; (b) **8** (*29*), 76%; (c) **9**, CAN, MeCN, −10 °C, 55%; (d) **10**, DMAP, NEt_3, CH_2Cl_2, $C_6H_5{}^{13}COCl$, 62%.

Electron Microscopy. Electron micrographs were obtained using a Hitachi 7000 TEM instrument. The samples were analyzed on 200 mesh hydrophilic carbon-coated grids and were stained with uranyl acetate.

RESULTS AND DISCUSSION

Synthesis of Paclitaxel Derivatives

The 3′-*N*-*m*-aminobenzoyl compound **2** was prepared in three steps in 66% overall yield from *N*-debenzoyl-2′-(triisopropylsilyl)paclitaxel (**4**) (*29*, *30*) by reaction with *m*-nitrobenzoyl chloride, deprotection of the 2′-TIPS group with HF/pyridine, and reduction of the NO_2 group with H_2/Pd-C in MeOH (Scheme 1).

The labeled compound **3** was prepared by using the β-lactam synthon method (*29*, *46*) to couple a suitably labeled β-lactam with a fluorinated baccatin III derivative. The key (3*R*,4*S*)-[^{15}N,4-^{13}C]-*N*-[*carbonyl*-^{13}C]benzoyl-3-[(triisopropylsilyl)oxy]-4-phenylazetidin-2-one (**11**) was prepared from [^{15}N]-*m*-anisidine (**7**) in four steps. Thus, the chiral enolate generated from (1*R*,2*S*)-*trans*-2-phenylcyclohexyl[(triisopropylsilyl)oxy]acetate and LDA in THF at −78 °C was treated with the labeled imine **8** to give the β-lactam **9** in 76% yield. Subsequent removal of the PMP group and acylation with [*carbonyl*-^{13}C]benzoyl chloride gave the triply labeled β-lactam **11** (Scheme 2).

[3′-^{13}C,^{15}N]-*N*-Debenzoyl-*N*-[*carbonyl*-^{13}C]benzoyl-2-debenzoyl-2-(*p*-fluorobenzoyl)paclitaxel (**3**) was synthesized by coupling the fluorobaccatin **14** [prepared by acylation of 2-debenzoyl-7,13-bis(triethylsilyl)baccatin III] and β-lactam **11**, followed by deprotection of the 2′-TIPS and 7-TES groups with HF/pyridine (Scheme 3).

Fluorescence Spectroscopy

Fluorescent Properties of N-AB-PT. *N*-AB-PT was synthesized as a fluorescent probe for the side chain region of

Scheme 3[a]

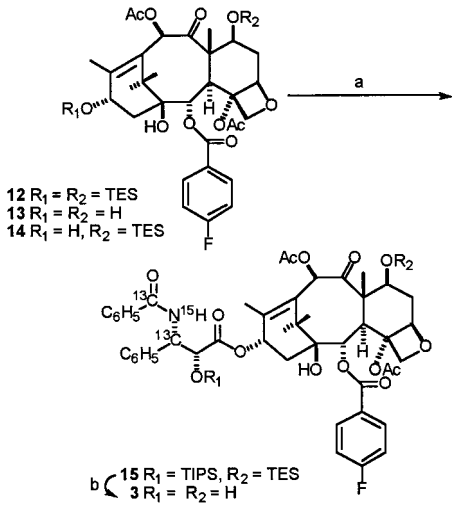

[a] (a) **11**, NaH, THF, 0 °C to room temperature, 72%; (b) HF/pyridine, 93%.

the paclitaxel binding site. The fluorophore was designed to be complementary to our previous fluorescent paclitaxel (*45*), in which the C-2 benzoate contained a *m*-amino group. Modifying the C-3′ benzamide in this manner had no detectable effect on the activity of the compound. The critical concentration of tubulin in the presence of either paclitaxel or *N*-AB-PT was identical within experimental error (data not shown). Since structure−activity studies show a wide variety of acceptable modifications in this region of paclitaxel (*47*, *48*), the minor modification was not expected to drastically alter the activity of the compound.

The fluorescence spectra of *N*-AB-PT in aqueous solution and bound to microtubules are illustrated in Figure 1. Microtubule binding induced a significant increase in the quantum yield of the drug (from 0.12 in buffer to 0.56 in the microtubule), and energy transfer from the protein to the drug was apparent.

The absorption and emission properties of *N*-AB-PT as a function of solvent were determined, and a Lippert plot (*49*) was constructed (Figure 2). In protic solvents, the Stokes shift of *N*-AB-PT increased with increasing solvent polarity. This result is expected with the *m*-aminobenzamide fluorophore. In aprotic solvents, however, the Stokes shift of the fluorophore was unaffected by the polarity of the solvent, which is not typical for the isolated fluorophore (*45*, *50*). It appears that the fluorophore is somehow "shielded" from the medium in aprotic solvents.

It was possible that the unusual spectroscopic behavior of *N*-AB-PT was the result of intermolecular hydrogen bonding in which the fluorophore was sequestered from the solvent. Evidence supporting such a solution structure for paclitaxel in an apolar solvent was suggested by Balasubramanian et al. from CD and NMR studies (*51*). We looked for evidence of self-association by examining the fluorescence emission spectrum of *N*-AB-PT in DMSO as a function of ligand concentration. No change in the shape of the spectrum or in the fluorescence emission maximum was observed for drug concentrations between 50 and 0.2 μM. The dimerization constant for *N*-AB-PT in DMSO would have to be $>10^7$ M^{-1} to be unobservable at such low concentrations. We therefore do not attribute the fluorescence data to intermolecular associations.

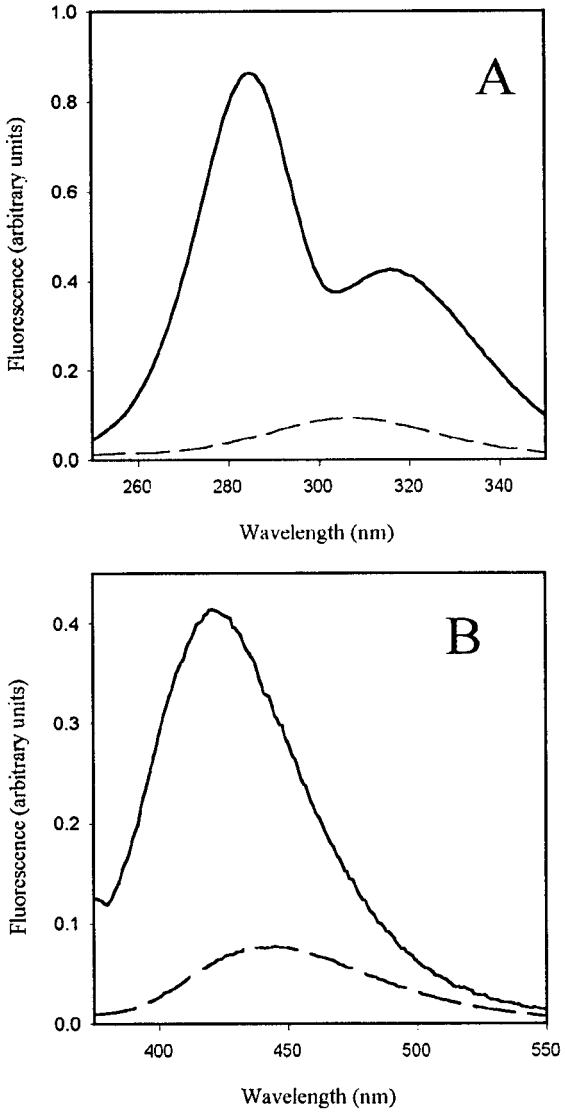

FIGURE 1: Excitation and emission spectra of *N*-AB-PT. (A) Excitation spectra of *N*-AB-PT. The lower curve is for 10 μM *N*-AB-PT in PMEG buffer containing 3% DMSO (emission wavelength of 446 nm). The upper curve is for microtubule-bound *N*-AB-PT, which was prepared by incubating 5 μM *N*-AB-PT with 10 μM tubulin in PMEG buffer for 20 min at room temperature (emission wavelength of 425 nm). (B) Emission spectra of *N*-AB-PT. The lower curve is for 10 μM *N*-AB-PT in PMEG buffer containing 3% DMSO. The emission maximum is 446 nm (excitation wavelength of 304 nm). The upper curve is for microtubule-bound *N*-AB-PT, which was prepared by incubating 5 μM *N*-AB-PT with 10 μM tubulin in PMEG buffer for 20 min at room temperature. The emission maximum is 424 nm (excitation wavelength of 325 nm).

These data can be explained by considering the conformational state of the taxoid. It is well-known that the conformation of the side chain varies with solvent (*17*, *18*). In aprotic solvents, the conformation generally resembles the X-ray structure of docetaxel (Figure 3, structure A), in which the 3′-benzamide is "under" the taxane ring and in the vicinity of the 2-benzoate, while the 3′-phenyl is extended into solution. In protic solvents, the relative positions of the 3′-phenyl and 3′-benzamide are reversed; the 3′-phenyl is now "under" the taxane ring, while the 3′-benzamide is extended into solution (Figure 3, structure B or C). Consider the environment a fluorophore at the 3′-benzamide position would experience in each conformation. In protic solvents,

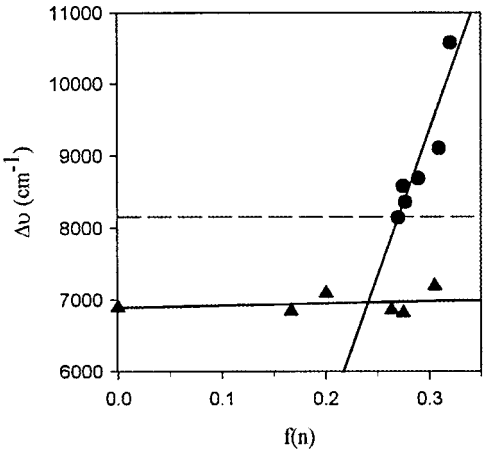

FIGURE 2: Effect of solvent polarity on the Stokes shift of *N*-AB-PT. The *f*(*n*) term is a measurement of solvent polarity (*49*): (▲) aprotic solvents (from left to right, hexane, diethyl ether, dioxane, ethyl acetate, dimethylformamide, DMSO, and acetonitrile), (●) protic solvents (from left to right, 2-butanol, 2-propanol, 1-propanol, ethanol, methanol, and 2% DMSO/H_2O), and (− − −) the Stokes shift of microtubule-bound *N*-AB-PT.

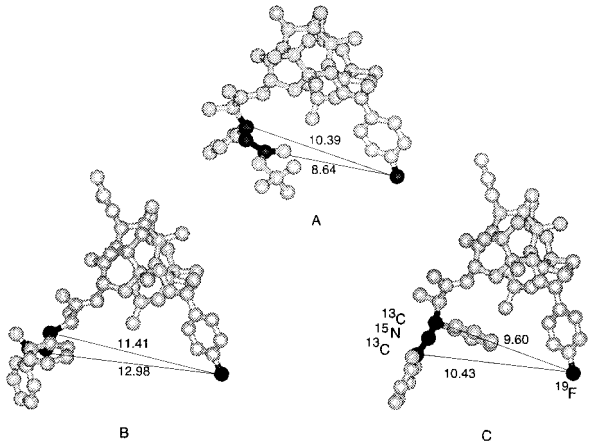

FIGURE 3: Possible conformations of microtubule-bound paclitaxel. Structure A is docetaxel using the X-ray coordinates (*16*). Two different conformations of paclitaxel were found in the crystal (*19*). Structure B corresponds to "Taxol A" and structure C to "Taxol B" in the original paper. ^{19}F, ^{15}N, and ^{13}C atoms are black. Distances between the nuclei used in REDOR are shown for each structure and were measured from the atomic coordinates of each molecule. Structure A illustrates the conformation of paclitaxel observed in aprotic solvents. Structure C most closely resembles one of the conformations of paclitaxel observed in protic solvents (*20*). No solution conformation corresponding to structure B has been reported.

the fluorophore is accessible to the medium and would be expected to display the normal solvent effects (structure C). In aprotic solvents, however, the fluorophore is contained within an intramolecular hydrophobic pocket (structure A). In the latter conformation, the environment of the fluorophore will consist mostly of taxoid atoms rather than solvent molecules, and would be invariable in the absence of a conformational change in the molecule. The possibility of intramolecular hydrogen bonding between the amide nitrogen and the C-2 carbonyl oxygen as an additional stabilizing interaction was not excluded by molecular mechanics. We therefore conclude that the Stokes shift of *N*-AB-PT in solvent reflects the conformational state of the molecule.

The Stokes shift of *N*-AB-PT bound to microtubules was clearly within the protic solvent region (dotted line in Figure 2). These data provide for the first time direct evidence that the microtubule-bound conformation of a paclitaxel derivative, and therefore paclitaxel itself, is the conformation of the molecule found in protic solvents.

A compound related to *N*-AB-PT, *N*-debenzoyl-*N*-[*m*-(dimethylamino)benzoyl]paclitaxel, has been previously reported and studied by Sengupta et al. (*52*, *53*). These investigators did not report the unusual spectroscopic behavior we observed with *N*-AB-PT. The Sengupta compound differs from *N*-AB-PT in that the amino group of the fluorophore is dimethylated; it is possible that the differences in the two sets of results are a consequence of the structural differences in the two paclitaxel derivatives.

Resonance Energy Transfer. Paclitaxel is but one of many natural products that associate with tubulin. Colchicine is representative of another class of antimitotic compounds that inhibit microtubule assembly through binding to the soluble tubulin heterodimer. The mechanism of colchicine binding to tubulin has been extensively investigated (*54*). The colchicine binding site on the protein has been assigned a portion of β-tubulin that is near the α,β-interface of the dimer from photoaffinity labeling and other experimental data. More recently, these data have been coupled with the electron diffraction structure of tubulin to provide a clearer indication of the colchicine receptor site on the protein (*55*).

The colchicine−tubulin complex can be induced to assemble into non-microtubule polymers that nevertheless have thermodynamic properties similar to those of microtubules (*56*). Paclitaxel will also induce tubulin liganded with colchicine to assemble into polymeric structures (*57*). In a previous study, we formed polymer sheets from tubulin liganded with a colchicine site drug and a fluorescent derivative of paclitaxel (*45*). By measuring fluorescence resonance energy transfer (RET) from the paclitaxel derivative to the colchicine site ligand, we determined that the C-2 position of paclitaxel is about 17 Å away from the colchicine binding site on tubulin when both are bound to the tubulin polymer. The same distance was obtained with a different acceptor in the colchicine site.

Since we were in possession of an active fluorescent paclitaxel with the fluorophore at a different site on the parent molecule, it was of interest to measure the distance between this fluorophore and the colchicine binding site. The distance distribution between the fluorophore in *N*-AB-PT and a ligand in the colchicine site (thiocolchicine) was measured in the same manner as described before on tubulin polymers formed with the two drugs (*45*). A distance of 29 Å with a distance distribution of 2 Å was found (Table 1).

Solid State NMR

NMR spectroscopy has been invaluable in the evaluation of paclitaxel conformations in solution (*14*, *17*, *18*, *23*, *58*−*62*). It has not been possible to apply the same techniques to studying microtubule-bound paclitaxel due to the large size of the receptor. Solid-state NMR techniques can be used on such systems, provided that the sample can be prepared in an appropriate form (*63*).

We have developed a method for preparing native paclitaxel-stabilized microtubules in the solid state (see Experimental Procedures). Solid samples of microtubules were routinely reconstituted and viewed by electron microscopy.

Table 1: Distances between the Colchicine C Ring and Two Paclitaxel Aromatic Rings in Different Paclitaxel Configurations

	distance (Å)			
	experimental[a]	system I[b,c]	system II[b,d]	system III[b,e]
C-2 benzoyl to the colchicine C ring	17 (3)[f,g]	25	25	17
C-3′ *N*-benzoyl to the colchicine C ring	29 (2)[g,h]	19	21	28

[a] Distance measured from fluorescence resonance energy transfer. [b] The position of colchicine was selected by docking the molecule to the atomic coordinates of tubulin prior to minimization, based on information in ref *55*. All distances were measured between the centers of the aromatic rings and the center of colchicine C ring. [c] The atomic coordinates from the diffraction data were used to position paclitaxel in the binding site prior to minimization. [d] Distance from paclitaxel in a conformation determined by fluorescence spectroscopy, in the original orientation within the binding site, to docked colchicine. [e] Distance from paclitaxel in a conformation determined by fluorescence spectroscopy, in an inverted conformation within the binding site, to docked colchicine. [f] From ref *35*. [g] Numbers in parentheses are the distance distributions. [h] From this work.

A majority of the structures observed in electron micrographs of the reconstituted sample were microtubules, indicating that microtubule structure was preserved in the solid state.

The paclitaxel molecule used in these experiments is **3** (Scheme 3, designated as 2-FB-PT). Internuclear distances between ^{19}F and ^{13}C were determined by REDOR as described in Experimental Procedures, and the results are shown in Figure 4. Assignments of the weak ^{13}C{^{19}F} REDOR difference peaks (Figure 4, top spectrum) were made by comparison to the isotropic peaks (and sidebands) in the ^{13}C{^{15}N} REDOR difference spectrum (Figure 4, middle). The signal:noise ratio for the ^{13}C{^{19}F} REDOR difference spectrum at the top of Figure 4 is only 3:1 at 175 ppm and 2:1 at 50 ppm. These values are determined with peak heights. The peak intensities, however, are determined with areas, and the integrals of the peaks have signal:noise ratios of about 5:1. An uncertainty in the intensity ratio of about 1 part in 5 (1 ± 0.2) translates into an uncertainty in the distance of about 6% (1 ± 0.06) because the distance has an inverse cube-root dependence on the extent of dipolar coupling, which is proportional to the intensity ratio. The accuracy of the distance determination is enhanced by the fact that the weak ^{13}C{^{19}F} REDOR difference peaks occur at the known frequencies of the stronger ^{13}C{^{15}N} REDOR difference spectrum (Figure 4, middle). Thus, the integrals for the distance determinations need to be performed over a limited frequency range. The distance between the C-3′ carbonyl carbon and C-2 *p*-fluorobenzoate fluorine was thus calculated to be 9.8 ± 0.5 Å, and that from the C-3′ methine carbon to the C-2 *p*-fluorobenzoate fluorine to be 10.3 ± 0.5 Å.

Three possible conformations for microtubule-bound paclitaxel are illustrated in Figure 3. Distances between the atoms used in REDOR were measured from the atomic coordinates of each structure (*16*, *19*), and these numbers are shown. On the basis of the REDOR results, it is clear that structure B cannot be the microtubule-bound conformation. But what cannot be determined with certainty is which of the two remaining conformations (structures A and C) is the microtubule-bound conformer.

We believe that the REDOR results support, but do not prove, that structure C best represents the microtubule-bound

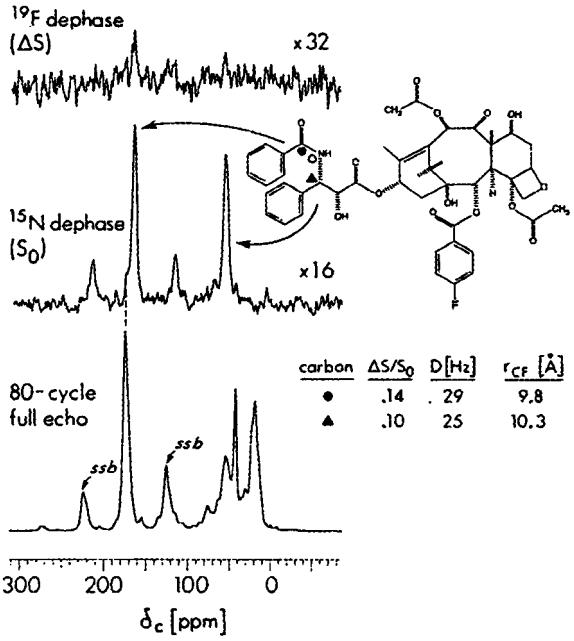

FIGURE 4: 125 MHz ^{13}C{^{15}N or ^{19}F} double REDOR spectra of 0.75 μmol of a 2-FB-PT (**3**)−microtubule complex stabilized in a poly(vinyl pyrrolidone) matrix with magic-angle spinning at 6.250 kHz. The full-echo spectrum after 80 rotor cycles is at the bottom of the figure. REDOR dephasing by ^{15}N generates a background-free spectrum from the two ^{13}C labels (middle). REDOR dephasing by ^{19}F generates a difference spectrum (top) whose intensities are interpreted quantitatively in terms of inter-ring distances (inset table). For this determination, the ^{13}C{^{15}N} REDOR difference spectrum is S_0 and the ^{13}C{^{19}F} REDOR difference spectrum is ΔS. The complete double REDOR experiment required the acquisition of 8 million scans (repetition period of 1 s) collected during a continuous 3 month period. The spinning speed and all four radiofrequency field amplitudes (H, F, C, and N) were under active control throughout this period.

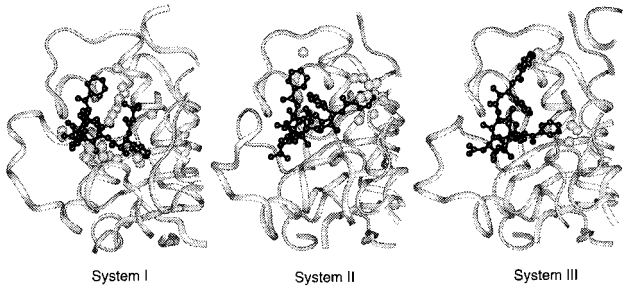

FIGURE 5: Possible orientations of paclitaxel bound to microtubules. The minimized structures of all orientations are shown. The initial conditions for the molecular mechanics calculations were as follows: system I, paclitaxel using atomic coordinates from Nogales et al. (*13*), modified as described in the text; system II, paclitaxel from the X-ray structure (Figure 4C) in the same orientation as in system I; and system III, paclitaxel from the X-ray structure (Figure 4C) in the "reversed" orientation. Atoms within 2 Å of any atom of the ligand are shown as gray balls.

conformer. This assertion arises from inspection of the differences between the distances from the crystal structures and from REDOR. For structure A, one REDOR distance matches the crystal distance (F to the methine carbon), but the other does not, although the discrepancy is not large. If structure A were the correct conformer, we would expect the methine and carbonyl carbon REDOR $\Delta S/S_0$ values to be dissimilar by a factor of about 2 rather than the observed factor of 1.4 (Figure 4). For structure C, both REDOR distances match the corresponding crystal distances within

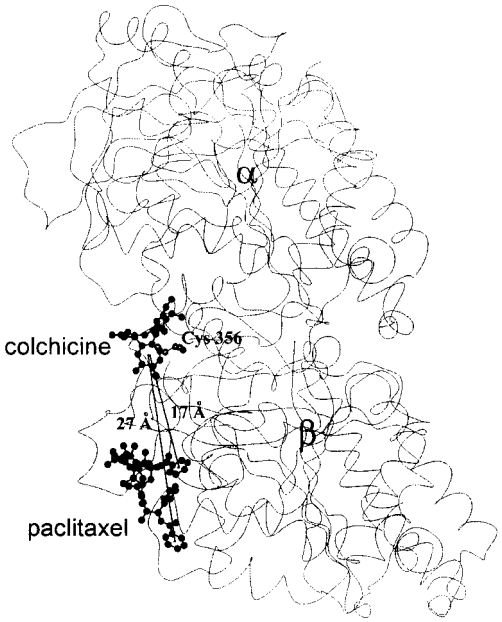

FIGURE 6: Relative positions of colchicine and paclitaxel bound to tubulin. Colchicine was docked into a putative binding site that is in agreement with a previous assignment (*55*) and available experimental data. Cys 356 of β-tubulin is highlighted for visual orientation. Paclitaxel is in the "reversed" orientation (Figure 5, system III), and the protein−paclitaxel complex has been minimized. The distances that are shown were measured between the center of the C ring of colchicine and the centers of the aromatic rings at C-2 and C-3′ of NHCOPh.

experimental error. However, in the crystal structure, the F to methine carbon distance is slightly shorter than the F to carbonyl carbon distance, whereas the REDOR distances are the other way around.

Because of this ambiguity, our assignment of the microtubule-bound structure of paclitaxel relies on both the fluorescence and REDOR data. The gross structural features of the microtubule-bound ligand, as indicated by a protic solvent Stokes shift, exclude structure A but not structures B and C. The REDOR high-resolution distances, on the other hand, exclude structure B but not structures A and C. Thus, the combined results of fluorescence and REDOR measurements identify structure C as the best representation of the conformation of paclitaxel when incorporated into microtubules.

Molecular Modeling

At least three different conformations of paclitaxel may represent the microtubule-bound conformer. REDOR NMR allowed us to eliminate one of these structures (structure B). Steady-state fluorescence spectroscopy data strongly indicate that the so-called hydrophobic collapsed conformation of paclitaxel (structure C) is the microtubule-bound form of the drug.

Merely substituting structure C for structure A in the paclitaxel binding site did not fit the totality of our data. According to our RET results, the C-2 phenyl ring should be closer to the colchicine binding site than the C-3′ NHCOPh ring. In fact, we found that this orientation of the structure was exactly the opposite of the orientation proposed from electron diffraction data (Table 1). The location of the colchicine binding site on the three-dimensional structure of tubulin has been assigned by analysis of the existing chemical and physical data (*55*), and the manual docking we performed was consistent with their assignment.

Molecular modeling was therefore employed to assist in visualizing the ligand−receptor complex. Three possible arrangements of the paclitaxel−tubulin complex were investigated. In system I (Figure 5), the coordinates from electron crystallography were chosen as the original structure. In system II, the appropriate coordinates from X-ray crystallography of paclitaxel were used for the starting structure. System III was formed on the basis of our fluorescence and REDOR results presented here. The tubulin-bound conformer of paclitaxel (structure C) was placed in the paclitaxel site in such a way as to interchange the C-2 and C-3′ NHCOPh aromatic rings. REDOR distances between the appropriate atoms were assigned as restraints, and each of the systems was minimized in a vacuum to obtain a three-dimensional representation of the possible receptor-bound ligand. The results are shown in Figure 5.

The minimized structures show that paclitaxel may be placed into the binding site in all three permutations. The distances between the centers of the C-2 and C-3′ NHCOPh aromatic rings and the center of the colchicine C ring were measured for the three scenarios (Table 1). The distances calculated for system III are well within the experimental error of the RET experiments (Figure 6).

Finally, we visually compared the characteristics of the calculated paclitaxel binding site with those from the diffraction structure. Photoaffinity labeling results put the C-2 aromatic ring in the proximity of β residues 217−231 and 337−350 and the C-3′ NHCOPh aromatic ring near β residues 1−31 (*64*, *65*). In our model, the C-3′ NHCOPh aromatic ring is close to β residues 225−229 and 19; the C-2 aromatic ring is close to β residues 229−233, 350, and 369. Interestingly, β residue His 229 minimizes to a position

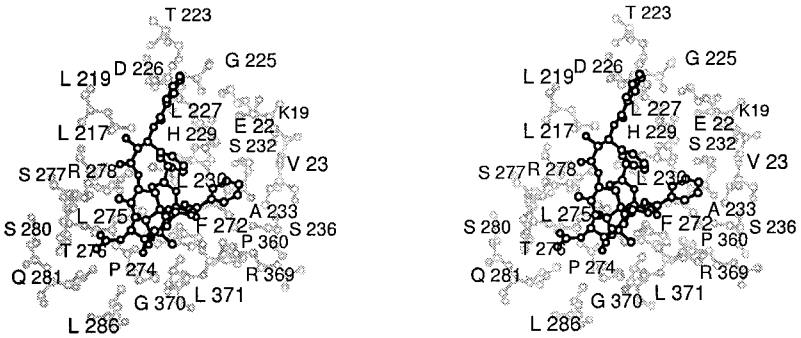

FIGURE 7: Stereoview of a model of paclitaxel bound to tubulin based on fluorescence and NMR data and on molecular modeling. Residues having atoms within 4 Å of any atom of the ligand are shown.

that is between these two phenyl rings. Our proposed structure is consistent with the photoaffinity labeling results but does not fit these data as well as the structure proposed by Nogales and Downing (*13*).

Two papers pertinent to our model have been published recently. Ojima et al. (*66*) and Wang et al. (*67*) have independently derived models for the paclitaxel pharmacophore. Both of these models fit known structure−activity data and are successful in predicting the activity of unknown compounds. Ojima et al. developed their model using solution-state NMR data for the structural template. The pharmacophore was derived on the basis of the topological homology of the ligands. Wang and Snyder used energy-minimized crystallographic structures as a starting point. A minireceptor, consisting of 20 amino acids of β-tubulin, was also constructed. The pharmacophore was developed on the basis of the goodness of fit to both ligand template and minireceptor. Interestingly, the conformation of paclitaxel is substantially different in the two models. Wang and Snyder started with the extended conformation of paclitaxel; the model in Ojima et al. uses a hydrophobic collapsed conformation of paclitaxel. Our results here are therefore more supportive of the model proposed by Ojima et al.

The minimized structure of system III that includes the protein residues with atoms within 4 Å of paclitaxel is illustrated in Figure 7, which we conclude represents the conformation and the orientation of microtubule-bound paclitaxel.

CONCLUSIONS

We have defined the conformation of microtubule-bound paclitaxel using two complementary methods. Information from steady-state measurements of fluorescence provided the gross structural features of the microtubule-bound molecule, specifically, that it is the hydrophobic collapsed conformer of paclitaxel. Solid-state NMR measurements provided two accurate distance measurements that served to further refine the structure of the tubulin-bound molecule. This information will be extremely useful in the design of future generations of paclitaxel-like drugs. For example, one can envision designing paclitaxels in which the side chain is conformationally restricted, which may increase the overall affinity of the drug for the receptor. This type of endeavor is presently being pursued in our laboratories.

We also propose an orientation for microtubule-bound paclitaxel that differs from the structure proposed from electron crystallography. Our RET distance measurements require the molecule be in this orientation, and its placement within the binding site in this manner is still consistent with photoaffinity labeling data. It will be interesting to see if our proposed model fits future, higher-resolution structural data.

NOTE ADDED IN PROOF

Molecular modeling studies with careful attention to the electron crystallography density have revealed a third "T-shaped" conformation of paclitaxel that is proposed to represent the microtubule-bound conformer (J. P. Snyder et al., submitted for publication). Our REDOR data are also consistent with this structure.

ACKNOWLEDGMENT

We thank Drs. Norman Camerman, Arthur Camerman, and Donald Mastropaolo for providing us with the coordinates for the two forms of paclitaxel. We are grateful to Dr. K. Downing and Dr. E. Nogales for providing the tubulin coordinates prior to their public release and to Dr. James P. Snyder for providing us a preprint of his manuscript. We thank Dr. James L. Potenziano, Jr., for technical assistance and discussion. We also thank P&N Packing for providing bovine brains.

SUPPORTING INFORMATION AVAILABLE

Full experimental details for the synthesis of compounds **2**−**14**. This material is available free of charge via the Internet at http://pubs.acs.org.

REFERENCES

1. Rowinsky, E. K. (1997) *Annu. Rev. Med. 48*, 353−374.
2. Von Hoff, D. D. (1997) *Semin. Oncol. 24*, S13-3−S13-10.
3. Eisenhauer, E. A., and Vermorken, J. B. (1998) *Drugs 55*, 5−30.
4. Goldspiel, B. R. (1997) *Pharmacotherapy 17*, 110S−125S.
5. Wiseman, L. R., and Spencer, C. M. (1998) *Drugs Aging 12*, 305−334.
6. Schiff, P. B., Fant, J., and Horwitz, S. B. (1979) *Nature 277*, 665−667.
7. Rodi, D. J., Janes, R. W., Sanganee, H. J., Holton, R. A., Wallace, B. A., and Makowski, L. (1999) *J. Mol. Biol. 285*, 197−203.
8. Landino, L. M., and Macdonald, T. L. (1995) *Pharmacochem. Libr. 22*, 301−335.
9. Horwitz, S. B. (1994) *Ann. Oncol. 5* (Suppl. 6), S3−S6.
10. Derry, W. B., Wilson, L., and Jordan, M. A. (1995) *Biochemistry 34*, 2203−2211.
11. Torres, K., and Horwitz, S. B. (1998) *Cancer Res. 58*, 3620−3626.
12. Ojima, I., Habus, I., Zhao, M., Zucco, M., Park, Y. H., Sun, C. M., and Brigaud, T. (1992) *Tetrahedron 48*, 6985−7012.
13. Nogales, E., Wolf, S. G., and Downing, K. H. (1998) *Nature 391*, 199−203.
14. Williams, H. J., Scott, A. I., Dieden, R. A., Swindell, C. S., Chirlian, L. E., Francl, M. M., Heerding, J. M., and Krauss, N. E. (1993) *Tetrahedron 49*, 6545−6560.
15. Milanesio, M., Ugliengo, P., and Viterbo, D. (1999) *J. Med. Chem. 42*, 291−299.
16. Guèritte-Voegelein, F., Guènard, F., Mangatal, L., Potier, P., Guilhem, J., Cesario, M., and Pascard, C. (1990) *Acta Crystallogr. C46*, 781−784.
17. Vander Velde, D. G., Georg, G. I., Grunewald, G. L., Gunn, C. W., and Mitscher, L. A. (1993) *J. Am. Chem. Soc. 115*, 11650−11651.
18. Paloma, L. G., Guy, R. K., Wrasidlo, W., and Nicolaou, K. C. (1994) *Chem. Biol. 1*, 107−112.
19. Mastropaolo, D., Camerman, A., Luo, Y., Brayer, G. D., and Camerman, N. (1995) *Proc. Natl. Acad. Sci. U.S.A. 92*, 6920−6924.
20. Ojima, I., Kuduk, S. D., Chakravarty, S., Ourevitch, M., and Begue, J. (1997) *J. Am. Chem. Soc. 119*, 5519−5527.
21. Kingston, D. G. I. (1991) *Pharmacol. Ther. 52*, 1−34.
22. Kingston, D. G. I. (1994) *Trends Biotechnol. 12*, 222−227.
23. Nicolaou, K. C., Dai, W.-M., and Guy, R. K. (1994) *Angew. Chem., Int. Ed. 33*, 15−44.
24. Hahn, K. M., Hastie, S. B., and Sundberg, R. J. (1992) *Photochem. Photobiol. 55*, 17−27.
25. Chabin, R. M., Feliciano, F., and Hastie, S. B. (1990) *Biochemistry 29*, 1869−1875.
26. Williams, R. C., Jr., and Lee, J. C. (1982) *Methods Enzymol. 85*, 376−385.
27. Detrich, H. W., III, and Williams, R. C., Jr. (1978) *Biochemistry 17*, 3900−3907.

28. Kingston, D. G. I., Chordia, M. D., Jagtap, P. G., Liang, J., Shen, Y.-C., Long, B. H., Fairchild, C. R., and Johnston, K. A. (1999) *J. Org. Chem. 64*, 1814−1822.
29. Ojima, I., Kuduk, S. D., Slater, J. C., Gimi, R. H., and Sun, C. M. (1996) *Tetrahedron 52*, 209−224.
30. Georg, G. I., Boge, T. C., Cheruvallath, Z. S., Harriman, G. C. B., Hepperle, M., and Park, H. (1994) *Bioorg. Med. Chem. Lett. 4*, 335−338.
31. Axenrod, T., Pregosin, P. S., Wieder, M. J., Becker, E. D., Bradley, R. B., and Milne, G. W. A. (1971) *J. Am. Chem. Soc. 93*, 6536−6541.
32. Lambert, J. B., and Stec, D., III (1984) *Org. Magn. Reson. 22*, 301−307.
33. Chen, S., Farina, V., Wei, J., Long, B., Fairchild, C., Mamber, S. W., Kadow, J. F., Vyas, D., and Doyle, T. W. (1994) *Bioorg. Med. Chem. Lett. 4*, 479−482.
34. Kingston, D. G. I., Chaudhary, A. G., Chordia, M. D., Gharpure, M., Gunatilaka, A. A. L., Higgs, P. I., Rimoldi, J. M., Samala, L., Jagtap, P. G., Giannakakou, P., Jiang, Y. Q., Lin, C. M., Hamel, E., Long, B. H., Fairchild, C. A., and Johnston, K. A. (1998) *J. Med. Chem. 41*, 3715−3726.
35. Han, Y., Malak, H., Chaudhary, A. G., Chordia, M. D., Kingston, D. G. I., and Bane, S. (1998) *Biochemistry 37*, 6636−6644.
36. Demas, J. M., and Crosby, G. A. (1971) *J. Phys. Chem. 75*, 991−1024.
37. Lakowicz, J. R., Gryvznski, I., Laczko, G., and Joshi, N. (1991) in *Luminescence Techniques in Chemical and Biochemical Analysis*, pp 141−177, Marcel Dekker, New York.
38. Lakowicz, J. R., Gryczynski, I., Wiczk, W., Kusba, J., and Johnson, M. L. (1991) *Anal. Biochem. 195*, 243−254.
39. Penefsky, H. A. (1977) *J. Biol. Chem. 252*, 2891−2899.
40. Beusen, D. D., McDowell, L. M., Slomczynska, U., and Schaefer, J. (1995) *J. Med. Chem. 38*, 2742−2747.
41. Gullion, T., and Schaefer, J. (1989) *Adv. Magn. Reson. 13*, 57−83.
42. Gullion, T., and Schaefer, J. (1989) *J. Magn. Reson. 81*, 196−200.
43. Goetz, J. M., Wu, J. H., Yee, A. F., and Schaefer, J. (1998) *Solid State Nucl. Magn. Reson. 12*, 87−95.
44. Gullion, T., Baker, D. B., and Conradi, M. S. (1990) *J. Magn. Reson. 89*, 479−484.
45. Han, Y., Chaudhary, A. G., Chordia, M. D., Sackett, D. L., Perez-Ramirez, B., Kingston, D. G., and Bane, S. (1996) *Biochemistry 35*, 14173−14183.
46. Holton, R. A., Biediger, R. J., and Boatman, P. D. (1995) in *Taxol: Science and Applications* (Suffness, M., Ed.) pp 97−121, CRC Press, Boca Raton, FL.
47. Georg, G. I., Boge, T. C., Cheruvallath, Z. S., Clowers, J. S., Harriman, G. C. B., Hepperle, M., and Park, H. (1995) in *Taxol: Science and Applications* (Suffness, M., Ed.) pp 317−375, CRC Press, Boca Raton, FL.
48. Kingston, D. G. I., Molinero, A. A., and Rimoldi, J. M. (1993) in *Progress in the Chemistry of Organic Natural Products* (Herz, W., Kirby, G. W., Moore, R. E., Steglich, W., and Tamm, C., Eds.) pp 1−206, Springer-Verlag, New York.
49. Lakowicz, J. R. (1983) in *Principles of Fluorescence Spectroscopy*, pp 189−215, Plenum Press, New York.
50. Koutek, B. (1978) *Collect. Czech. Chem. Commun. 43*, 2368−2386.
51. Balasubramanian, S. V., Alderfer, J. L., and Straubinger, R. M. (1994) *J. Pharm. Sci. 83*, 1470−1476.
52. Sengupta, S., Boge, T. C., Georg, G. I., and Himes, R. (1995) *Biochemistry 34*, 11889−11894.
53. Sengupta, S., Boge, T. C., Liu, Y., Hepperle, M., Georg, G. I., and Himes, R. H. (1997) *Biochemistry 36*, 5179−5184.
54. Hastie, S. B. (1991) *Pharmacol. Ther. 51*, 377−401.
55. Downing, K. H., and Nogales, E. (1998) *Eur. Biophys. J. 27*, 431−436.
56. Andreu, J. M., Wagenknecht, T., and Timasheff, S. N. (1983) *Biochemistry 22*, 1556−1566.
57. Howard, W. D., and Timasheff, S. N. (1988) *J. Biol. Chem. 263*, 1342−1346.
58. Hilton, B. D., Chmurny, G. N., and Muschik, G. M. (1992) *J. Nat. Prod. 55*, 1157−1161.
59. Chmurny, G. N., Hilton, B. D., Brobst, S., Look, S. A., Witherup, K. M., and Beutler, J. A. (1992) *J. Nat. Prod. 55*, 414−423.
60. Dubois, J., Guenard, D., Gueritte-Voeglein, F., Guedira, N., Potier, P., Gillet, B., and Betoeil, J.-C. (1993) *Tetrahedron 49*, 6533−6544.
61. Williams, H. J., Scott, A. I., Dieden, R. A., Swindell, C. S., Chirlian, L. E., Francl, M. M., Heerding, J. M., and Krauss, N. E. (1994) *Can. J. Chem. 72*, 252−260.
62. Jimenez-Barbero, J., Souto, A. A., Abal, M., Barasoain, I., Evangelio, J. A., Acuna, A. U., Andreu, J. M., and Amat-Guerri, F. (1998) *Bioorg. Med. Chem. 6*, 1857−1863.
63. McDowell, L. M., and Schaefer, J. (1996) *Curr. Opin. Struct. Biol. 6*, 624−629.
64. Rao, S., Krauss, N. E., Heerding, J. M., Swindell, C. S., Ringel, I., Orr, G. A., and Horwitz, S. B. (1994) *J. Biol. Chem. 269*, 3132−3134.
65. Rao, S., Orr, G. A., Chaudhary, A. G., Kingston, D. G. I., and Horwitz, S. B. (1995) *J. Biol. Chem. 270*, 20235−20238.
66. Ojima, I., Chakravarty, S., Inoue, T., Lin, S., He, L., Horwitz, S. B., Kuduk, S. D., and Danishefsky, S. J. (1999) *Proc. Natl. Acad. Sci. U.S.A. 96*, 4256−4261.
67. Wang, M., Xia, X., Kim, Y., Hwabng, D., Janmsen, J. M., Liotta, D. C., and Snyder, J. P. (1999) *Org. Lett. 1*, 43−46.

BI991936R